PHYSICAL REVIEW A **85**, 031803(R) (2012)

Excitability and self-pulsing in a photonic crystal nanocavity

Maia Brunstein,[1,*] Alejandro M. Yacomotti,[1,†] Isabel Sagnes,[1] Fabrice Raineri,[1] Laurent Bigot,[2] and Ariel Levenson[1]

[1]*Laboratoire de Photonique et de Nanostructures (CNRS UPR 20), Route de Nozay, Marcoussis F-91460, France*

[2]*Laboratoire de Physique des Lasers, Atomes et Molécules (CNRS UMR8523), Université Lille1 IRCICA, 50 avenue Halley, F-59658 Villeneuve d'Ascq Cedex, France*

(Received 21 October 2011; published 26 March 2012)

Bistability, excitability, and self-pulsing regimes in an InP-based two-dimensional (2D) photonic crystal nanocavity with quantum wells as an active medium are investigated. A resonant cw beam is evanescently coupled into the cavity through a tapered microfiber. In such conditions, we show that the cavity exhibits class II excitability, which arises from the competition between a fast electronic nonlinear effect, given by carrier-induced refractive index change, and slow thermal dynamics. Multiple perturbation-pulse experiments allow us to measure the refractory time ("dead time" between two excitable pulses) of the excitable nanocavity system.

DOI: 10.1103/PhysRevA.85.031803 PACS number(s): 42.70.Qs, 05.45.−a, 42.60.Da

Among the great diversity of nonlinear processes in optics, nonlinear dynamical phenomena such as bistability and excitability have recently received considerable attention. While bistability is well known as a building block for all-optical memories, switching, and logic gates, excitability underlies spiking behavior to external stimuli. This has been originally introduced in neuroscience as the mechanism responsible for action potential firing in neurons [1]. In optics, excitability has been mainly studied in active resonators. First demonstrated in a semiconductor laser under optical feedback [2], it has been recently investigated in microphotonics and nanophotonics, namely in a two-dimensional (2D) photonic crystal band-edge resonator, where it has been identified as thermo-optical excitability [3]. More recently, a fascinating example of excitability has been reported in the context of optomechanics: the optical torque wrench [4]. Importantly, an excitable system may undergo a transition to self-sustained oscillations as long as a control parameter is varied.

Fast third-order nonlinearity is the key element to achieve the above-mentioned regimes in an optical cavity. These effects being generally weak, their enhancement is of central importance to reduce operation thresholds. For instance, nonlinear effects can be enhanced in systems allowing tight light confinement and low optical loses, such as photonic crystal (PhC) nanocavities. According to [5,6], a reduction of both the optical volume and optical losses leads to a decrease of the bistability threshold since the latter scales as V/Q^2, with V the optical mode volume and Q the cavity quality factor. So far, only few works were devoted to the understanding and implementation of nonlinear dynamics in PhC nanocavities. They have mostly focused on the optical bistability of thermal origin, mainly because thermal effects in ultra-small cavities are usually dominant against ultra-fast nonlinearities. Electronic nonlinearities in nanoresonators are more difficult to achieve and observe due to both technological issues and the small signals in play with fast time scales (picosecond to nanosecond). Even so, some works have recently demonstrated the bistability of electronic origin in PhC nanocavities [7,8].

Excitability is usually defined in a phenomenological way [9]: a small perturbation from the stable state can result in a large and long-lasting excursion of the physical variables before the system comes back to equilibrium. Furthermore, as an external parameter is changed, the global attractor in the form of the stationary point may bifurcate into a stable periodic orbit, and the excitability behavior undergoes oscillatory dynamics. In particular, in the so-called class II excitability, dynamical regimes involve variables with different time scales: a fast one, responsible for the firing of the excitable pulse, and a slow one, which determines the full recovery to the quiescent state [10]. In semiconductor materials, the fast dynamical variable is given by the carrier density and the slow one by the temperature. Within a cavity, the fast time scale is usually given by the carrier recombination time [11] since the field variables adiabatically follow the evolution of the other (much slower) ones; the slow time scale is governed by the thermal relaxation due to thermal diffusion [12]. In standard resonators, as the one used in [13], the thermal relaxation time is of the order of a millisecond. In microresonators such as microdisks or photonic crystals, this time scale can be much shorter due to the small dimensions involved in heat diffusion [14].

These nonlinear scenarios, such as excitability, have already been investigated in PhC extended resonators [3]. However, they have never been reported in PhC cavities. Recently, theoretical predictions of self-pulsing in microcavities and nanocavities have been carried out [15–17]. In this work, we demonstrate self-sustained oscillations and excitable regimes in an InP-based PhC nanocavity.

The 2D PhC used in this work is a triangular array of air holes etched into a 10×50 μm InP-based suspended membrane. The period and the hole radius are $a = 450$ nm and $r = 120$ nm, respectively. An L3 nanocavity (three missing holes) with the two end holes shifted away by $0.15a$ to increase the quality factor [18] is located in the center of the 2D PhC [Fig. 1(a)]. The suspended InP membrane (265-nm thick, $\lambda/2n$), grown by metalorganic vapor phase epitaxy (MOCVD), incorporates four central layers of InGaAs/InGaAsP quantum

*Present address: Paris Descartes University, 45 Rue des Saints Pères F-75270 Paris Cedex 06, France.

†alejandro.giacomotti@lpn.cnrs.fr

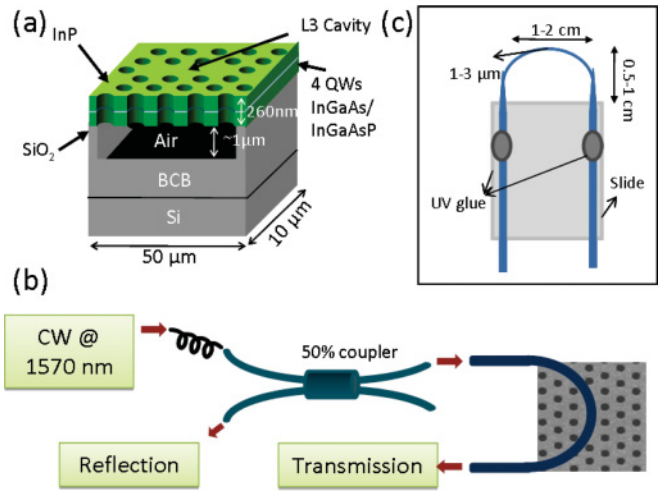

FIG. 1. (Color online) (a) Schematic of the PhC sample showing the L3 cavity. The InP is bonded onto a silicon substrate through a SiO_2–benzocyclobutene (BCB) layer; the SiO_2 is subsequently removed to obtain a suspended membrane. (b) Tapered fiber optical coupling scheme for transmission and reflectivity measurements. A Scanning Electron Microscopy (SEM) image of the L3 cavity is shown. (c) Sketch of the tapered fiber characteristics.

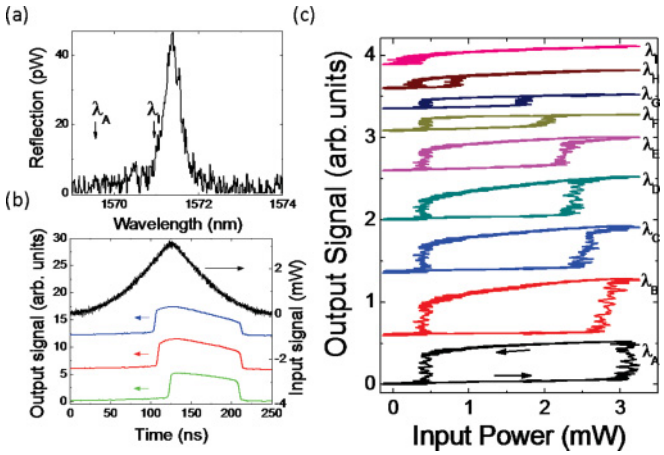

FIG. 2. (Color online) (a) Reflected signal for a probe power of 95 μW. Arrows λ_A to λ_I indicate the wavelength range for the bistability experiment. (b) Time traces of input [black (top) line (right vertical axis)] and reflected [blue, red, and green lines (left vertical axis)] signals for detunings of $\Delta\lambda = 1.5$, 1.7, and 1.9 nm, respectively. (c) Hysteresis cycles showing bistable behavior. Detuning values with respect to the cavity resonance are, from λ_A to λ_I, 1.9, 1.8, 1.7, 1.5, 1.3, 1.1, 0.9, 0.7, and 0.4 nm. The input power is measured at the tapered fiber input. The durations of the switch processes is ~6 ns for the on and off switches.

wells (QWs), whose luminescence at 300 K is centered around 1.51 μm.

Due to the highly noncircular lobes in the radiation patterns of L3 cavities [19], coupling light from free space is inefficient. Thus, the characterization of the cavity mode and the nonlinear measurements are performed by evanescently coupling a signal into the nanocavity through a tapered optical fiber [Fig. 1(b)]. The tapered fiber (diameter of ~ 1.5 μm) is bent [Fig. 1(c)] in such a way that the curved segment approaches the PhC. Such a U-shaped configuration reduces contact losses (leakage and absorption) in the substrate. The incident polarization angle can be changed by means of a fiber polarization controller. To probe the cavity mode, a 30-nm broadband signal (120-fs width, 80-MHz repetition rate optical parametric oscillator) with a central wavelength of 1570 nm is coupled into the cavity. An estimation of the coupling efficiency (η) can be obtained from the ratio of the transmitted signal "in" (T_{in}) and "out" (T_{out}) of resonance [12] in the following way: $\eta = 1 - \sqrt{T_{\text{in}}/T_{\text{out}}}$, which gives ~7%.

The cavity mode couples to the fiber mode in both directions. The backward signal is measured in reflection using a 50% fibred coupler [Fig. 1(b)]. From now on, all signals will be measured at the reflection port of the fiber. The reflected signal is shown in Fig. 2(a): a mode centered at $\lambda = 1571.4$ nm with a loaded quality factor of $Q_{\text{loaded}} = 3752$ is observed. The intrinsic cavity Q factor can be deduced from Q_{loaded} and η as $Q_0 = Q_{\text{loaded}}/(1-\eta) \sim 4030$. Note that Q_0 results from both optical and absorption losses. In a similar sample with negligible absorption we typically obtain intrinsic Q factors of about 6300, which quantify the optical quality of our L3 cavities, limited by fabrication imperfections.

A fast nonlinear response can be obtained as a result of carrier-induced refractive index change in the cavity [20]. This blue-shifts the resonance as a function of the injected power, which changes the intensity of single-wavelength reflection or transmission signals to the output ports [11]. In particular, a bistable operation [21] is observed for the range of wavelengths shown in Fig. 2(a) as 3.2-mW peak power, 250-ns-width triangular pulses are sent to the cavity through the tapered fiber [Fig. 2(b)]. Figure 2(c) shows the hysteresis cycles for different detuning values, $\Delta\lambda = \lambda_0 - \lambda_{\text{inj}}$, with λ_0 and λ_{inj} the resonance and injected wavelengths, respectively. Note the existence of the two bistable branches: the high and low reflectivity (upper and lower) states, respectively. The input power-bistability threshold is $P_{\text{input,th}} = 300$ μW for a normalized detuning of $|\delta_0| = |\lambda_0 - \lambda_{\text{inj}}|/\gamma \sim 1.9$, where γ is the half-width of the resonance [Fig. 2(c), top curve]. Considering the fiber losses, this corresponds to a power in the vicinity of the cavity of $P_{\text{in,th}} \sim 170$ μW. From this value, the intrinsic (i.e., the power coupled into the cavity) threshold can be estimated as $P_{\text{th}}^{\text{expt}} = \eta P_{\text{in,th}} \sim 12$ μW. This value is close to previously reported power thresholds [7,8].

From a theoretical point of view, the intrinsic threshold can be approximated by $P_{\text{th}} \sim |\delta_0| P_0^{(\text{elec})}$, with $P_0^{(\text{elec})}$ the characteristic (electronic) nonlinear power [6]. In the case of index nonlinearities driven by carrier-induced one-photon absorption in the QWs, this is given by

$$P_0^{(\text{elec})} = \frac{\hbar\omega_0^3 N_t}{2\Gamma v_{g0}^2 \tau_{\text{nr}} \alpha_0^2 \alpha_H} \frac{V_{\text{cav}}}{Q^2} \tag{1}$$

with $v_{g0} \sim c/3$ the group velocity of the homogeneous membrane, ω_0 the resonance frequency, $\tau_{\text{nr}} \sim 200$ ps the nonradiative recombination time [20], $\Gamma \sim 0.2$ the confinement factor, $\alpha_0 \sim 54\,\text{cm}^{-1}$ the unsaturated absorption, $N_t \sim 10^{18}\,\text{cm}^{-3}$ the carrier density at transparency, $\alpha_H \sim 10$ the Henry factor, and

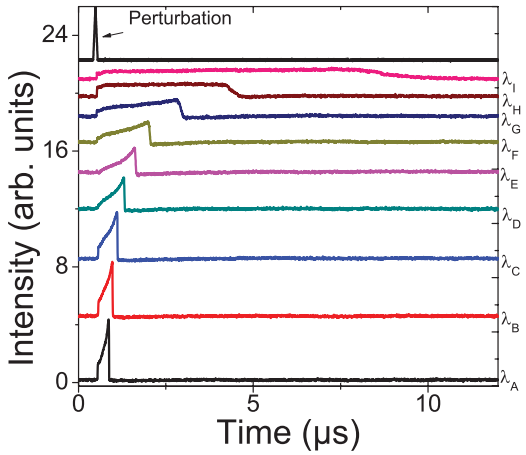

FIG. 3. (Color online) Transient responses (bottom traces) for different detunings. The detunings (in nanometers) and the injected powers (in megawatts) are, from λ_A to λ_I, 1.8 and 2.9; 1.7 and 2.5; 1.6 and 2.2; 1.5 and 1.8; 1.4 and 1.6; 1.3 and 1.3; 1.2 and 1.2; 1.1 and 0.9; 1 and 0.8. The top trace corresponds to the perturbation signal (peak power = 80 μW).

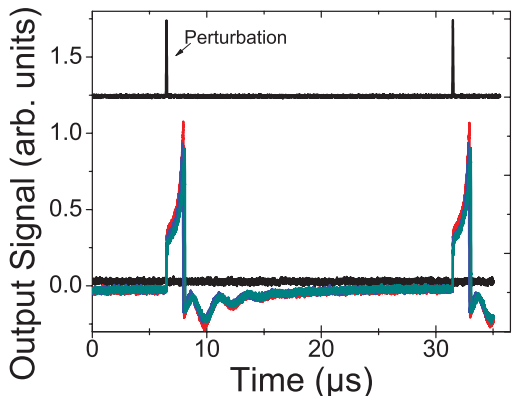

FIG. 4. (Color online) Excitable responses (bottom traces) to 130-ns width, 40-KHz repetition rate pulse perturbations (top trace) for different perturbation powers: 1 μW is below threshold (black line); 20, 35, and 46 μW are above threshold [red, blue, and green lines, respectively (gray lines)]. The injected signal power is set at 2.6 mW and the detuning is $\Delta\lambda = 1.5$ nm.

$V_{\text{cav}} \sim 0.08\ \mu\text{m}^3$ [22] the mode volume. Note the explicit factor V/Q^2 in Eq. (1). We also point out that P_0 is the intrinsic power level that shifts the resonance about one half-width; with these parameters we obtain $P_0^{(\text{elec})} \sim 4\,\mu$W. In terms of threshold values, using $|\delta_0| = 1.9$, we get $P_{\text{th}}^{\text{theo}} \sim 7.6\,\mu$W, which is roughly a factor of 2 smaller than the experimental value. Such a difference can be attributed to the error bars of the estimated or calculated parameters, as well as to additional losses not taken into account.

In bistability experiments, the signal modulation minimizes thermal effects. Turning off the modulation, thermal loading plays an important role. This is shown in Fig. 3, where a cw signal is injected in such a way that both the lower and upper states of Fig. 2 coexist. Now the system is switched from the lower to the upper states by introducing a short perturbation. This is achieved injecting 130-ns-width, 40-kHz repetition rate incoherent pulses with $\lambda = 808$ nm. The perturbation beam, incident from the free space, is focused down using a long working distance, 50 × microscope objective to a diameter of $\sim 4\,\mu$m. Once switched to the upper state, there is a transient period where the reflected signal remains high, and it eventually drops back to the lower state. The perturbation power has been fixed in such a way that switching from the lower to the upper state is ensured for all detuning values.

Importantly, a shrinking of the transient response with increasing detuning is observed. Indeed, two behaviors can be distinguished: a fast and well-contrasted response, or "pulse," and a slow and quasistationary one. The fast and well-contrasted response occurs for both high detuning and injected powers (Fig. 3, λ_A to λ_D). Slow, quasi-cw bistability with less contrasted jumps occur for both low detuning and injected signals (Fig. 3, λ_G to λ_I). The longest memory time that has been obtained is about $\sim 8\,\mu$s in such a case. The physical mechanism responsible for these transient outputs is the cavity heating. This can be quantified through the

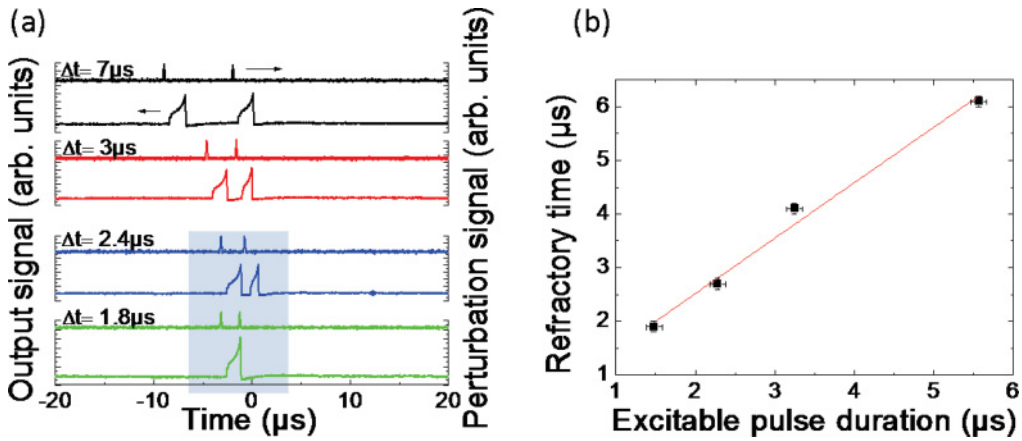

FIG. 5. (Color online) (a) Output and perturbation signals (lower and upper traces) as a function of time for different delays (Δt) between 808-nm perturbation pulses; $\Delta\lambda = 1.2$ nm, injected power 2.8 mW, and perturbation power 255 μW. The refractory time is $\sim 2\,\mu$s, determined as Δt just before the two output pulses take place (in between the two highlighted situations). (b) Refractory time as a function of the excitable pulse duration ($\Delta\lambda = 1.2$, 1.1, 1, and 0.9 nm for increasing excitable pulse duration). (Red) line: linear fit.

characteristic intrinsic power for thermal effects

$$P_0^{(\text{thermal})} = \frac{c\omega_0\rho C_p}{4\Gamma v_{g0}^2 \tau_{\text{dis}} \alpha_0 (dn/dT)} \frac{V_{\text{cav}}}{Q^2}, \tag{2}$$

where C_p is the heat capacity, ρ the mass density ($\rho C_p \sim 1.5\,\text{Jcm}^{-3}\text{K}^{-1}$), $\tau_{\text{dis}} \sim 185$ ns the thermal diffusion time of the cavity and $dn/dT \sim 1.9 \times 10^{-4}\,\text{K}^{-1}$ the thermal index change [12]. These parameters yield $P_0^{(\text{thermal})} \sim 2\,\mu$W. The fact that $P_0^{(\text{thermal})} \lesssim P_0^{(\text{elec})}$ explains that thermal effects cannot be neglected in this case. Moreover, they are at the origin of the transient phenomena observed. A purely electronic effect could be expected in the opposite limit [i.e., as long as $P_0^{(\text{thermal})} \gg P_0^{(\text{elec})}$].

In all the situations depicted in Fig. 3, the system is injected with powers above the bistability threshold; therefore, a steady state on the upper branch of the hysteresis cycle can be expected to exist. However, heating is enhanced in such conditions, increasing the refractive index and thus shifting the hysteresis cycle to higher injection powers. As a result, a self-induced switch to the low reflectivity state takes place, with a subsequent cooling, giving rise to a two-time-scale transient response [3]: fast jumps are governed by carrier effects, while the slow dynamics determining the pulse duration is ruled by thermal effects.

We now focus on the pulsed output regime. This takes place, for instance, for $\Delta\lambda = 1.5$ nm. Setting the injection power to 2.6 mW, the system is stable, the steady state corresponding to a small reflected power level. In such conditions, the cavity is likely to show excitable behavior. This can be tested by injecting perturbation pulses with different amplitudes. Figure 4 shows the reflected signal as a function of time. For perturbation powers lower than 1 μW, no output pulse is observed (black line). As the perturbation power is increased to 20 μW, a 2-μs-duration output pulse is observed. The pulse features remain essentially invariant for a further increase of the perturbation. Thus, a calibrated pulsed response takes place with a 20-μW threshold. These are clear signatures of the excitable behavior of the system. Moreover, the optical response shows a slow ($\sim$1 μs due to thermal effects) and a fast (in the ns scale, driven by electronic effects) dynamics which builds confidence on class II excitability.

Let us discuss the power balance between the incoming and outgoing pulses. As the InP absorption coefficient at 810 nm is $\sim$33%, and considering the cavity surface with respect to the excitation area, the absorbed power in the cavity is reduced to $\sim$0.7 μW for a 20-μW incoming pulse. On the other hand, the peak power of the outgoing excitable pulse in the vicinity of the cavity is $\sim$1 μW. Therefore, no significant loss or amplification of the input perturbation energy takes place. However, we point out that increasing the coupling efficiency (η) and/or decreasing the excitable threshold may improve the power balance.

An important characteristic of the excitable phenomenon is the existence of a "dead time" between two successive events, called refractory time. This is defined as the time it takes for an excitable system to be ready for a second stimulus once it returns to its resting state. To experimentally investigate this feature, two perturbation pulses are sent to the sample and the optical response is studied as a function of the delay (Δt) between them. The refractory time is thus approximated as the minimum Δt for which two consecutive responses take place. Figure 5(a) shows the reflected signal and the perturbation signal as a function of time for four different Δt and $\Delta\lambda = 1.2$ nm: the refractory time is $\sim 2\,\mu$s. Figure 5(b) shows the refractory time for different $\Delta\lambda$: the excitable pulse duration is the pulse width of the response pulse for each detuning. Note that Fig. 5(a) illustrates the process for the determination of the first data point in Fig. 5(b) with an excitable pulse duration of 1.5 μs. It is found that the dependency of the refractory time upon the excitable pulse duration is linear. Further theoretical work is necessary to understand this linear scaling. The refractory time has been studied in detail in neurons, where it lies in the microsecond range. In optics, it has been previously investigated in a laser system [23].

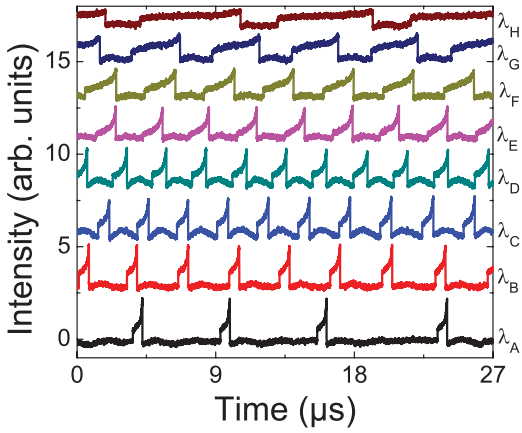

FIG. 6. (Color online) Self-sustained oscillations. Reflected signals as a function of time for different detunings, from λ_A to λ_H, 1.8, 1.7, 1.6, 1.5, 1.4, 1.3, 1.2, and 1.1 nm. The input power, measured at the tapered fiber input, is 3.2 mW.

It is worth pointing out that the excitable dynamics takes place close to the onset of self-sustained oscillations. Taking $\Delta\lambda = 1.5$ nm, in the absence of any perturbation, the system becomes self-pulsing above $\sim$ 2.9 mW. In general, self-sustained oscillations are observed for larger injection powers than those for which the system is excitable (Fig. 6), where no stable state exists: a periodic signal takes place, the frequency being governed by thermal effects. Note that the pulse period and width depend on both the injected power and the detuning. Details on fast and slow limit cycle dynamics can be found in [3].

In conclusion, we have experimentally demonstrated excitability and self-pulsing in a 2D PhC nanocavity. These nonlinear dynamical regimes have been achieved through a competition between electronic and thermal nonlinear responses. The excitable pulses showed a duration in the time scale of the thermal processes ($\sim$1 μs) while the rise time was of the order of the switching times found for the electronic bistability (nanosecond time scale). In addition, the refractory time was investigated and a linear dependency between

this time and the pulse duration was found. These results might open a door to future applications of active photonic crystal nanocavities as integrated networks of nonlinear optical cells.

These results are within the scope of C'Nano IdF and were supported by the Région Ile-de-France. C'Nano IdF is a CNRS, CEA, MESR and Région Ile-de-France Nanosciences Competence Center.

[1] A. L. Hodgkin and A. F. Huxley, J. Physiol. **117**, 500 (1952).
[2] M. Giudici, C. Green, G. Giacomelli, U. Nespolo, and J. R. Tredicce, Phys. Rev. E **55**, 6414 (1997).
[3] A. M. Yacomotti, P. Monnier, F. Raineri, B. B. Bakir, C. Seassal, R. Raj, and J. A. Levenson, Phys. Rev. Lett. **97**, 143904 (2006).
[4] F. Pedaci, Z. Huang, M. van Oene, S. Barland, and N. H. Dekker, Nat. Phys. **7**, 259 (2011).
[5] E. Centeno and D. Felbacq, Phys. Rev. B **62**, R7683 (2000).
[6] M. Soljačić, M. Ibanescu, S. G. Johnson, Y. Fink, and J. D. Joannopoulos, Phys. Rev. E **66**, 055601 (2002).
[7] M. K. Kim, I. K. Hwang, S. H. Kim, H. J. Chang, and Y. H. Lee, Appl. Phys. Lett. **90**, 161118 (2007).
[8] M. Notomi, T. Tanabe, A. Shinya, E. Kuramochi, H. Taniyama, S. Mitsugi, and M. Morita, Opt. Express **15**, 17458 (2007).
[9] A. Rabinovitch and I. Rogachevskii, Chaos: An Interdisciplinary Journal of Nonlinear Science **9**, 880 (1999).
[10] F. Hoppensteadt and E. M. Izhikevich, *Weakly Connected Neural Networks* (Springer, New York, 1997).
[11] M. Brunstein, A. M. Yacomotti, R. Braive, S. Barbay, I. Sagnes, L. Bigot, L. Le-Gratiet, and J. A. Levenson, IEEE Photonics Journal **2**, 642 (2010).
[12] M. Brunstein *et al*., Opt. Express **17**, 17118 (2009).
[13] S. Barland, O. Piro, M. Giudici, J. R. Tredicce, and S. Balle, Phys. Rev. E **68**, 036209 (2003).
[14] V. Moreau, G. Tessier, F. Raineri, M. Brunstein, A. Yacomotti, R. Raj, I. Sagnes, A. Levenson, and Y. De Wilde, Appl. Phys. Lett. **96**, 091103 (2010).
[15] B. Maes, M. Fiers, and P. Bienstman, Phys. Rev. A **80**, 033805 (2009).
[16] S. Malaguti, G. Bellanca, A. de Rossi, S. Combrié, and S. Trillo, Phys. Rev. A **83**, 051802 (2011).
[17] V. Grigoriev and F. Biancalana, Phys. Rev. A **83**, 043816 (2011).
[18] Y. Akahane, T. Asano, B.-S. Song, and S. Noda, Nature (London) **425**, 944 (2003).
[19] M. Brunstein, T. J. Karle, I. Sagnes, F. Raineri, J. Bloch, Y. Halioua, G. Beaudoin, L. L. Gratiet, J. A. Levenson, and A. M. Yacomotti, Appl. Phys. Lett. **99**, 111101 (2011).
[20] F. Raineri, C. Cojocaru, P. Monnier, A. Levenson, R. Raj, C. Seassal, X. Letartre, and P. Viktorovitch, Appl. Phys. Lett. **85**, 1880 (2004).
[21] A. M. Yacomotti *et al*. , Appl. Phys. Lett. **88**, 231107 (2006).
[22] A. R. A. Chalcraft *et al*. , Appl. Phys. Lett. **90**, 241117 (2007).
[23] J. R. Tredicce, AIP Conf. Proc. **548**, 238 (2000).